Design of Transmission Fibers and Doped Fiber Amplifiers for Mode-Division Multiplexing

Daulet Askarov and Joseph M. Kahn, *Fellow, IEEE*

***Abstract*— Transmission fibers and erbium-doped fiber amplifiers (EDFAs) for 12 signal modes (including spatial and polarization degrees of freedom) are studied. Modal fields are computed numerically and their effective areas, group delays (GDs), and chromatic dispersion coefficients are determined. Multimode rate equations are solved numerically to calculate mode-dependent gains (MDGs) and pump power requirements in multimode EDFAs. Results are compared for various numerical apertures (NAs), index profiles, and doping profiles. Graded-index depressed-cladding fibers offer an attractive combination of low GD spread in transmission fibers (583 ps/km rms with 0.15 NA) and low MDG in EDFAs (0.14 dB rms at 25-dB mode averaged gain with 0.15 NA). Optimized erbium doping profiles are comprised of a uniform cylindrical region plus an extra annulus.**

***Index Terms*— Multiplexing, optical fibers, optical fiber amplifiers.**

I. Introduction

As LONG-HAUL single-mode fiber systems approach information-theoretic limits [1], spatial multiplexing in multimode or multi-core fibers offers a possible route to higher throughput [2]–[4]. The properties of transmission fibers and fiber amplifiers are crucial to the feasibility of spatially multiplexed long-haul systems [5]. In transmission fibers, low group delay (GD) spread and mode-dependent chromatic dispersion (MDCD) minimize receiver signal processing complexity [6], [7], while large modal effective areas minimize nonlinear effects. In fiber amplifiers, low mode-dependent gain (MDG) minimizes the loss of capacity and the potential for outage [8]. In this letter, we jointly study multimode transmission fibers and multimode EDFAs (MM-EDFAs) for spatial multiplexing in 12 modes (including spatial and polarization degrees of freedom), considering different numerical apertures (NAs) and refractive index profiles. While our previous work [9] used scalar wave equations, here we use vector wave equations to find modal fields and evaluate GD spreads, modal effective areas and MDCD in transmission fibers. By solving multimode rate equations, we evaluate MDGs and power conversion efficiencies of MM-EDFAs.

Manuscript received July 31, 2012; revised September 4, 2012; accepted September 7, 2012. Date of publication September 28, 2012; date of current version October 15, 2012. This work was supported in part by the National Science Foundation under Grant ECCS-1101905 and in part by Corning, Inc.

The authors are with the Department of Electrical Engineering, E. L. Ginzton Laboratory, Stanford University, Stanford, CA 94305-4088 USA (e-mail: daskarov@stanford.edu; jmk@ee.stanford.edu).

Color versions of one or more of the figures in this letter are available online at http://ieeexplore.ieee.org.

Digital Object Identifier 10.1109/LPT.2012.2218654

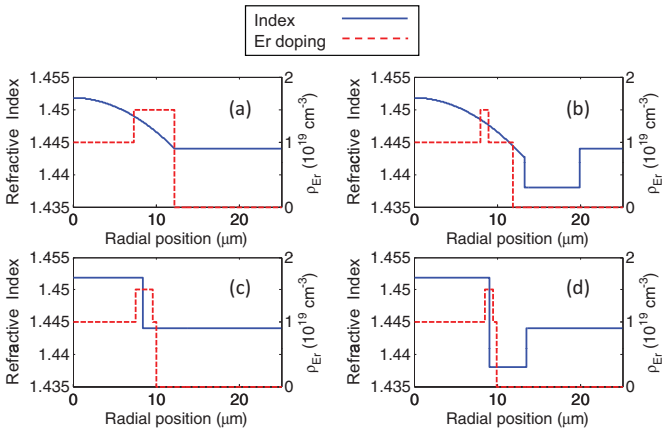

Fig. 1. Refractive index and Er doping profiles for fibers with numerical aperture NA = 0.15. (a) GI. (b) GIDC. (c) SI. (d) SIDC.

II. Design and Modeling Methodology

A. Transmission Fibers

We consider the four types of refractive index profiles shown in Fig. 1(a-d): (a) graded-index (GI), (b) graded-index with depressed cladding (GIDC), (c) step-index (SI) and (d) step-index with depressed cladding (SIDC), for NAs ranging from 0.1 to 0.2. At each NA, we adjust the core radius, as described in Section III below, to support a total of 12 propagating signal modes, which include non-degenerate TE_{01} and TM_{01} modes and doubly degenerate HE_{11}, HE_{21}, EH_{11}, HE_{31} and HE_{12} modes.

We use a vector mode solver [10] to find the field distributions and propagation constants of the modes without assuming weak guidance. Given the field pattern $\mathbf{E}$ of a particular mode, we compute the effective area using

$$A_{eff} = \frac{(\int |E|^2 dA)^2}{\int |E|^4 dA}$$

integrating over the fiber cross section. To characterize the dispersion of a particular mode, we expand the propagation constant as a function of frequency

$$\beta(\omega) \approx \beta_0 + \beta_1 \cdot (\omega - \omega_0) + \frac{1}{2}\beta_2 \cdot (\omega - \omega_0)^2.$$

We numerically estimate the first and second derivatives of the propagation constant by slightly changing the wavelength and using the vector mode solver to find the corresponding change in propagation constant, thereby obtaining the GD per unit length β_1 and the chromatic dispersion (CD) parameter β_2.

We use the Sellmeier equation [11] to take into account the dispersion of the Ge-doped silica in the core, the F-doped silica in the depressed cladding and the pure silica in the outer cladding.

B. Fiber Amplifiers

For each NA and index profile type, we design the MM-EDFA to have refractive index profile identical to the transmission fiber. We consider two types of Er doping profiles. The first is uniform over a disk, and the second is uniform with an extra annulus. For each fiber design, we optimize the doping profile, as described in Section III below, to minimize MDG assuming end pumping with equal power in each pump mode. Fig. 1(a-d) show uniform doping profiles with the extra annulus that have been optimized for the corresponding index profiles.

Bi-directional, mode-scrambled, dual-polarization end pumping through dichroic couplers would facilitate the high pump powers required for multiple modes and wavelengths. Here we model the simpler case of a co-propagating pump, in order to speed up simulations and facilitate exploration of a wide range of design parameters.

We numerically compute the vector fields of signal and pump modes without assuming weak guidance. Assuming a three-level model, neglecting inhomogeneous broadening and amplified spontaneous emission, we generalize the amplifier power rate equations [12] to multiple signal and pump spatial modes

$$\frac{dP_{s,k}}{dz} = P_{s,k}\int_0^{2\pi}\int_0^{r_d}\Big[\sigma_e(\lambda_s)N_2(r,\varphi,Z) - \sigma_a(\lambda_s)N_1(r,\varphi,Z)\Big]\Big|\Psi_{s,k}(r,\varphi)\Big|^2 r\,dr\;d\varphi$$

$$\frac{dP_{p,l}}{dz} = -P_{p,l}\sigma_a(\lambda_p)\int_0^{2\pi}\int_0^{r_d} N_1(r,\varphi,z)\Big|\Psi_{p,l}(r,\varphi)\Big|^2 r\,dr\;d\varphi.$$

Here, $P_{s,k}(z)$ and $P_{p,l}(z)$ describe the evolution of the kth signal mode ($k = 1,\ldots,k_{\max}$) at wavelength λ_s, and of the lth pump mode ($l = 1,\ldots,l_{\max}$) at wavelength λ_p, respectively over amplifier length z; $\Psi_{s,k}(r,\varphi)$ and $\Psi_{p,l}(r,\varphi)$ are the corresponding normalized vector electric field distributions; r_d is the maximal radius at which the fiber in MM-EDFA is doped; and $\sigma_a(\lambda)$ and $\sigma_e(\lambda)$ denote the wavelength-dependent absorption and emission cross sections of Er ions, respectively. The local concentrations of Er ions at lower and upper energy levels $N_1(r,\varphi,z)$ and $N_2(r,\varphi,z)$ are functions of Er doping distribution $N_{Er}(r)$, and local signal and pump intensities

$$N_1(r,\varphi,z) = N_{Er}(r)\left(1+\frac{\sigma_e(\lambda_s)}{\sigma_e(\lambda_s)+\sigma_a(\lambda_s)}\frac{I_s(r,\varphi,z)}{I_{s,sat}}\right)\times\left(1+\frac{I_s(r,\varphi,z)}{I_{s,sat}}+\frac{I_p(r,\varphi,z)}{I_{p,sat}}\right)^{-1}$$

$$N_2(r,\varphi,z) = N_{Er}(r) - N_1(r,\varphi,z)$$

each normalized to saturation intensities at the corresponding wavelengths

$$I_{s,sat} = hc/[\lambda_s(\sigma_a(\lambda_s)+\sigma_e(\lambda_s))]$$
$$I_{p,sat} = hc/[\lambda_p\sigma_a(\lambda_p)].$$

The local signal and pump intensities, in turn, are given by

$$I_s(r,\varphi,z) = \left|\sum_K \sqrt{P_{s,k}(z)}e^{-j\beta_k z + j\theta_{s,k}}\Psi_{s,k}(r,\varphi)\right|^2$$

$$I_p(r,\varphi,z) = \left|\sum_l \sqrt{P_{p,l}(z)}e^{-j\beta_l z + j\theta_{p,l}}\Psi_{p,l}(r,\varphi)\right|^2$$

Here, $\theta_{s,k}$ and $\theta_{p,l}$ are the initial phases of the signal and pump modes at the input end of the amplifier.

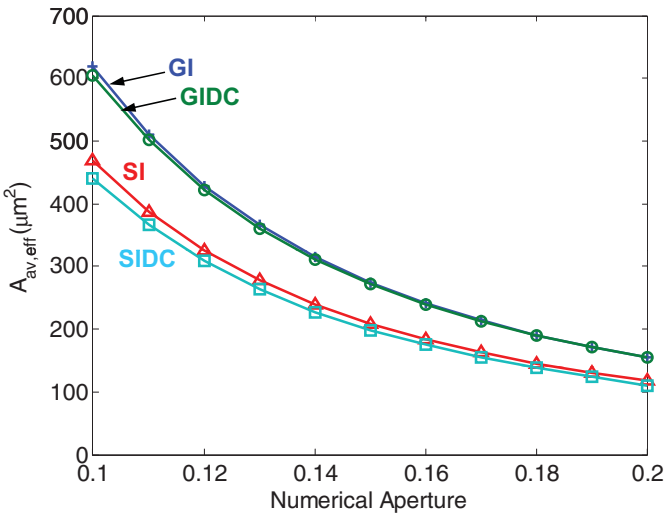

Fig. 2. Average effective mode area in fiber with 12 modes as a function of numerical aperture for different refractive index profiles.

III. Simulation Results

For a given index profile type and NA, there is a range of core radii supporting the desired 12 propagating signal modes. We choose the core radius such that at the shortest wavelength of the C-band (1530 nm), the next higher-order mode is slightly above cutoff. While maintaining 12 signal modes over the C-band, this optimizes modal confinement, minimizing bending losses and minimizing MDG and MDCD. In the GIDC and SIDC index profiles, we choose the outer radius of the DC to be 1.5 times the inner core radius.

Fig. 2 shows modal effective areas averaged over the 12 signal modes for different index profiles. Lower NAs lead to larger effective areas, since the core radius is larger. Also, GI and GIDC fibers have larger mode effective areas than SI and SIDC fibers; when maintaining 12 propagating modes with the next higher-order mode near cut-off, the modes in step-index fibers are more confined than those in graded-index fibers. At this design point, GIDC fibers support 42 pump modes, while GI, SI and SIDC fibers support 34 pump modes.

Fig. 3 shows peak-to-peak and root-mean-square (rms) GD spreads among the 12 propagating modes. For all fibers, the peak-to-peak and rms spreads have almost the same dependence on NA, except for a factor of about three. Lower NAs

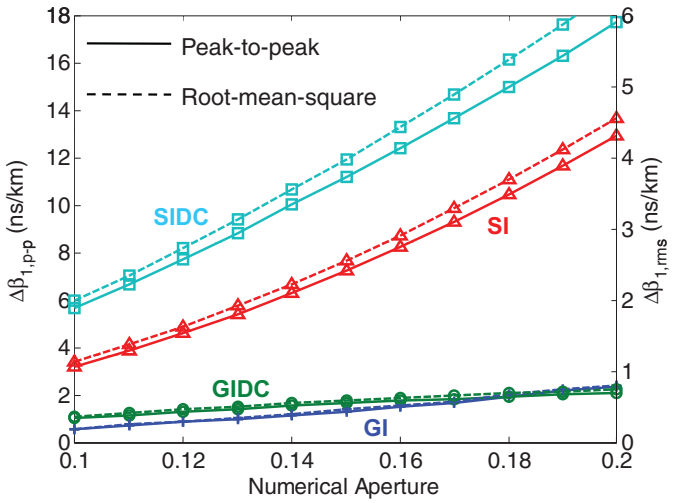

Fig. 3. Peak-to-peak and root-mean square group delay per unit length for modes in 12-mode fiber as a function of numerical aperture for different refractive index profiles.

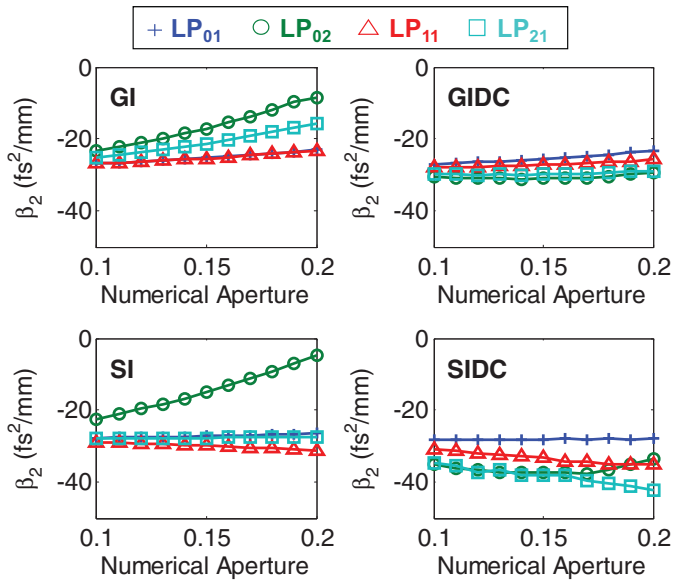

Fig. 4. Chromatic dispersion of modes in 12-mode fibers grouped by LP mode groups as a function of numerical aperture for different refractive index profiles.

yield lower GD spreads, while GI and GIDC fibers have lower GD spreads than SI and SIDC fibers, as expected [13].

Fig. 4 shows CD parameters for fibers of different index profiles and NAs. Because the fibers considered are weakly guiding, the CD parameter is nearly the same for all vector modes within an LP mode group. Thus, modes are sorted here according to LP mode groups [14]. Fibers with depressed cladding have lower MDCD, owing to more uniform confinement across the different mode groups.

In MM-EDFAs, we choose the uniform disk and extra annulus (when present) to have doping concentrations of 1.0 and 1.5×10^{19} cm^{-3}, respectively. We avoid higher doping levels to prevent pair-induced quenching [15]. We first optimize the uniform disk radius r_d to minimize MDG, assuming equal power in each pump mode. We then add the extra annulus and adjust its inner and outer radii to minimize MDG.

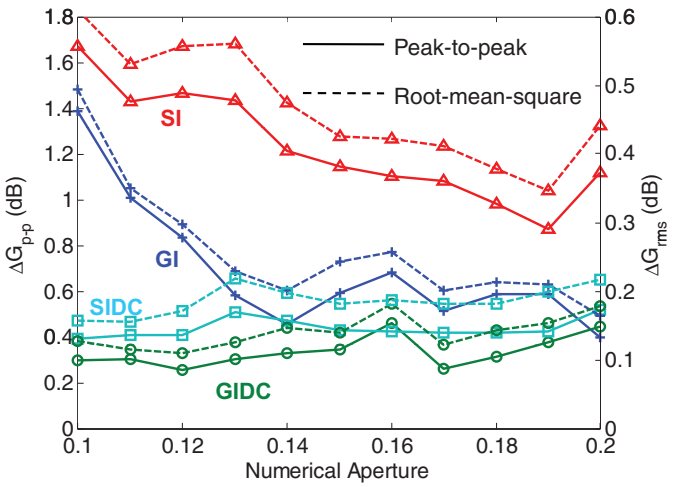

Fig. 5. Peak-to-peak and root-mean-square MDG of 12 modes in MM-EDFA averaged over 16 random phase combinations of input signal and pump modes as a function of NA for different index profiles. The pump power is chosen such that the mode-averaged gain is 25 dB. The uniform doping profile with extra annulus is optimized at each NA.

In modeling the MM-EDFAs, we assume a continuous-wave input signal at a single wavelength $\lambda_s = 1550$ nm, with equal input powers in the 12 modes, chosen so the total output signal power is 0.6 W. This output power corresponds to wavelength-division multiplexing of 100 signals, each with 0.5 mW output power per spatial mode per polarization. We assume a pump at $\lambda_p = 980$ nm, with equal power in all pump modes, and adjust the total pump power to obtain a mode-averaged signal gain of 25 dB. We choose the amplifier length as the value of z at which the amplified signal power reaches its maximum, thereby minimizing the required pump power.

Fig. 5 shows the peak-to-peak and rms MDG for different index profiles and NAs, each data point averaged over 16 random combinations of input signal and pump mode phases $\theta_{s,k}$ and $\theta_{p,l}$. Three trends are evident. First, fibers with depressed cladding have lower MDG, presumably because better mode confinement enhances spatial overlap between signal and pump modes. Second, in SI and GI fibers, MDG is observed to decrease at higher NAs. As the NA is increased, the core radius must be decreased to support a fixed number of signal modes, increasing local intensities at a given total signal power. This leads, in turn, to higher and more uniform inversion over the doped region, which may reduce MDG. Third, GI/GIDC fibers have lower MDG than their SI/SIDC counterparts. This may be caused by differences in modal propagation constants or field patterns, but requires further study. Fig. 6 shows the pump power required for 0.6-W total output signal power and 25-dB average signal gain. As the NA varies from 0.1 to 0.2, required pump powers range from 1.7 to 1.0 W for SI or SIDC fibers and from 2.1 to 1.2 W for GI or GIDC fibers. These correspond to power conversion efficiencies ranging from 35 to 60% for SI or SIDC fibers, and from 29 to 50% for GI or GIDC fibers. The higher efficiencies observed in SI/SIDC or higher-NA fibers are due to smaller mode effective areas and, as a result, higher local intensities and inversion levels given the same total power.

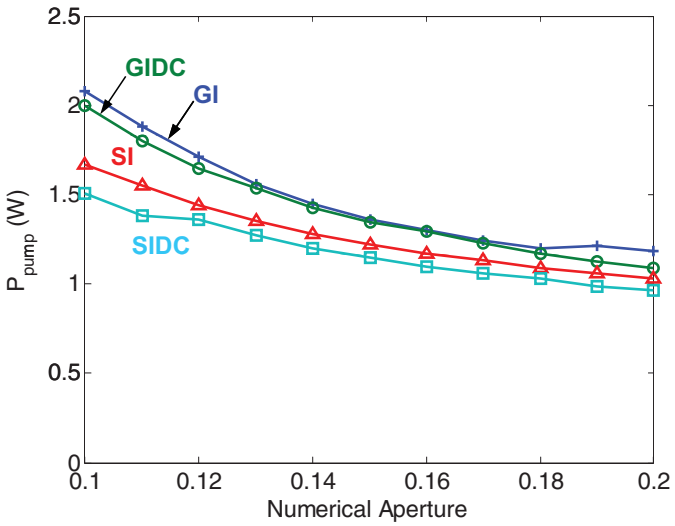

Fig. 6. Input pump power at $\lambda_p = 980$ nm, which is required for 25-dB average signal gain and 0.6-W total output signal power in 12-mode MM-EDFA as a function of numerical aperture for different refractive index profiles.

IV. Conclusion

GIDC or SIDC index profiles are clearly superior to their non-DC counterparts because better confinement of higher-order modes (especially HE_{12}) significantly reduces MDG and MDCD. For all fiber designs, the extra doping annulus is highly beneficial, reducing the rms dB values of MDG by about fourfold. The choice of NA, like the choice between GI/GIDC and SI/SIDC, is less obvious, because as these are varied, important fiber and amplifier properties exhibit conflicting trends. Effective areas are larger and GD spreads are smaller at low NAs, and for GI/GIDC profiles. By contrast, amplifier pumping efficiencies are higher at high NAs and for SI/SIDC profiles.

GD spread is important in mode-division-multiplexed (MDM) systems because it affects the complexity of digital signal processing (DSP) used to compensate modal dispersion and separate multiplexed signals [7]. Early MDM experiments [16] have used step-index fibers supporting six modes in two polarizations (three spatial modes in two mode groups). In these fibers, the NA and core radius can be chosen for low GD spread, even when fibers have little or no mode coupling. In fibers supporting more than six modes, it is not clear how to obtain such low GD spreads, and our GIDC 12-mode fibers have rms GD spreads about 11 to 22 times higher than the SI six-mode fibers of [16]. When using fibers with more than six modes, as argued in [7], strong mode coupling may be used to reduce the GD spread and thus ensure that DSP complexity is manageable. In the strong coupling regime, the rms GD spread scales with the square-root of fiber length [6], and the statistics of the coupled GDs depend on the uncoupled GDs (those shown in Fig. 3) only through the rms value [6].

MDG is critical in MDM systems because excessive MDG can reduce capacity and lead to outage [8]. In a system with cascaded amplifiers, strong mode coupling can reduce the accumulated MDG. In the strong-coupling regime, the accumulated MDG scales with the square-root of the number of amplifiers, and the statistics of the coupled MDG depend on the uncoupled MDGs (those shown in Fig. 5) only through the rms value measured in dB [8]. The low values of MDG for fibers with optimized index and doping profiles shown in Fig. 5 would result in minimal performance degradation, even in systems with tens of cascaded amplifiers [8].

In estimating the MDG we have assumed equal power in each pump mode, a condition that may be difficult to satisfy. Hence, active control of MDG, for example, as in [17], may be required in practice.

References

[1] R.-J. Essiambre, G. Kramer, P. J. Winzer, G. J. Foschini, and B. Goebel, "Capacity limits of optical fiber networks," *J. Lightw. Technol.*, vol. 28, no. 4, pp. 662–701, Feb. 15, 2010.

[2] H. R. Stuart, "Dispersive multiplexing in multimode optical fiber," *Science*, vol. 289, no. 5477, pp. 281–283, 2000.

[3] A. Tarighat, R. C. J. Hsu, A. Shah, A. H. Sayed, and B. Jalali, "Fundamentals and challenges of optical multiple-input multiple-output multimode fiber links," *IEEE Commun. Mag.*, vol. 45, no. 5, pp. 57–63, May 2007.

[4] A. R. Shah, R. C. J. Hsu, A. Tarighat, A. H. Sayed, and B. Jalali, "Coherent optical MIMO (COMIMO)," *J. Lightw. Technol.*, vol. 23, no. 8, pp. 2410–2419, Aug. 2005.

[5] T. Morioka, Y. Awaji, R. Ryf, P. Winzer, D. Richardson, and F. Poletti, "Enhancing optical communications with brand new fibers," *IEEE Commun. Mag.*, vol. 50, no. 2, pp. s31–s42, Feb. 2012.

[6] K.-P. Ho and J. M. Kahn, "Statistics of group delays in multimode fiber with strong mode coupling," *J. Lightw. Technol.*, vol. 29, no. 21, pp. 3119–3128, Nov. 1, 2011.

[7] S. O. Arik, D. Askarov, and J. M. Kahn, "Effect of mode coupling on signal processing complexity in mode-division multiplexing," *J. Lightw. Technol.*, to be published.

[8] K.-P. Ho and J. M. Kahn, "Mode-dependent loss and gain: Statistics and effect on mode-division multiplexing," *Opt. Express*, vol. 19, no. 17, pp. 16612–16635, Aug. 2011.

[9] D. Askarov and J. M. Kahn, "Design of multi-mode erbium-doped fiber amplifiers for low mode-dependent gain," in *Proc. IEEE Photon. Soc. Summer Topical Space Division Multiplex. Opt. Syst. Netw.*, Seattle, WA, Jul. 2012, pp. 1–2.

[10] S. Dods, "Fiber vector modesolver–improvements to the efficient 4×4 matrix method," in *Tech. Dig. Integr. Photon. Res. Appl./Nanophoton.*, 2006, pp. 1–3.

[11] S. Kasap and P. Capper, *Springer Handbook of Electronic and Photonic Materials*. Berlin, Germany: Springer-Verlag, 2007.

[12] E. Desurvire, *Erbium-Doped Fiber Amplifiers: Principles and Applications*. New York: Wiley, 1994.

[13] K. Okamoto, *Fundamentals of Optical Waveguides*. New York: Academic, 2006.

[14] J.-R. Qian and W.-P. Huang, "LP modes and ideal modes on optical fibers," *J. Lightw. Technol.*, vol. 4, no. 6, pp. 626–630, Jun. 1986.

[15] P. Myslinski, D. Nguyen, and J. Chrostowski, "Effects of concentration on the performance of erbium-doped fiber amplifiers," *J. Lightw. Technol.*, vol. 15, no. 1, pp. 112–120, Jan. 1997.

[16] R. Ryf, *et al.*, "Mode-division multiplexing over 96 km of few-mode fiber using coherent 6×6 MIMO processing," *J. Lightw. Technol.*, vol. 30, no. 4, pp. 521–531, Feb. 15, 2012.

[17] N. Bai, E. Lp, T. Wang, and G. Li, "Multimode fiber amplifier with tunable modal gain using a reconfigurable multimode pump," *Opt. Express*, vol. 19, no. 17, pp. 16601–16611, 2011.